Synchrotron X-ray Renninger scanning for studying strain in InAs/GaAs quantum dot system

Raul O. Freitas, Tómas E. Lamas, Andre A. Quivy, and **Sérgio L. Morelhão***

Instituto de Física, Universidade de São Paulo, CP 66318, 05315-970 São Paulo, Brazil

Key words Nanostructured devices, quantum dots, semiconductors, x-ray diffraction, synchrotron radiation.
PACS 61.10.Nz; 61.10.Dp

A systematic procedure for ultra-precise lattice parameter determination using x-ray Renninger scanning (XRS) is optimized and applied to probe the average in-plane strain in series of samples representing the different stages of the growth process of single-buried quantum dots (QDs). Covering InAs QDs growth on GaAs (001) substrates generates an expansive in-plane strain that is related to the density of QDs. Rocking curves and atomic force microscopy are also used for a general qualitative analysis of the growths, as well as of the morphology and density of the QDs.

1 Introduction

Synchrotron radiation has become an indispensable tool in many fields of Materials Science. Several analytical techniques are so important that most synchrotron facilities have stations optimized for carrying out specific techniques routinely. Systematic procedures for data acquisition and data treatment are also necessary mainly in studies involving large ensembles of samples, as for instance when developing new materials and nanostructured devices for technological applications.

X-ray Renninger scanning (XRS) is one of the most accurate techniques for absolute lattice parameter determination in single crystal [1, 2, 3, 4, 5, 6, 7]. However, in despite of this fact, there still are major limitations for systematically using XRS in studying technological materials: *i)* difficulties experimented by users not familiar with multi-beam diffraction geometry in choosing suitable $umwegs$ for a given purpose — $umweg$, a short name for the multi-beam diffraction peaks in the XRS — ; *ii)* instrumental errors that compromise accuracy in studies where it is really necessary; *iii)* lack of simple line-profile functions capable of measuring peak positions without further reducing accuracy due to the usually asymmetrical profiles of the $umwegs$; and *iv)* the need of a package of standardized procedures to handle quickly and systematically the materials analysis in synchrotron facilities.

Opto-electronic devices based on self-organized InAs quantum dots (QDs) on GaAs substrates have wavelength emission range suitable for application in metropolitan-area networks [8]. An actual challenge for practical usage of these devices resides in increasing their optical efficiency, which is possible by covering the previously grown QDs by a few atomic GaAs layers, and thus providing a new surface for the growth of more QDs. However, drastic reductions in the number of optically active structures after covering are in general observed. Since surface probe techniques are no longer useful to inspect the physical structure of buried QDs; alternative structural characterization procedures have become relevant.

In this work, a systematic procedure [9] for ultra-precise lattice parameter determination using XRS is optimized and applied to probe the average in-plane strain in series of samples representing the different stages of the growth process of single-buried QDs. This procedure takes advantage of the shallow

* Corresponding author: e-mail: morelhao@if.usp.br, Phone: +55 11 3091 6807, Fax: +55 11 3091 6749

penetration depth of the X-ray wavefield under Bragg-surface diffraction [10, 11] — a particular type of $umweg$ — , to enhance the sensitivity to the in-plane strain closer to the surface. Mechanical imprecision and residual sample-misalignment errors are treated automatically, and a genetic algorithm plus a phase sensitive line-profile function [12] are employed for fast and accurate peak position measurements.

2 Theoretical aspects

X-ray multi-beam diffraction in crystals are excited when the incident beam, wavevector $\boldsymbol{k}$, fulfill two Bragg conditions

$$\boldsymbol{k}\cdot\boldsymbol{P} = -\boldsymbol{P}\cdot\boldsymbol{P}/2 = -|\boldsymbol{k}||\boldsymbol{P}|\sin\theta_P \qquad \text{and} \tag{1}$$

$$\boldsymbol{k}\cdot\boldsymbol{S} = -\boldsymbol{S}\cdot\boldsymbol{S}/2 = -|\boldsymbol{k}||\boldsymbol{S}|\sin\theta_S. \tag{2}$$

Since $\boldsymbol{P}=\boldsymbol{S}+\boldsymbol{C}$ we also have

$$\boldsymbol{k}\cdot\boldsymbol{C} = -\boldsymbol{C}\cdot\boldsymbol{C}/2 - \boldsymbol{C}\cdot\boldsymbol{S} \tag{3}$$

where $\boldsymbol{P}$, $\boldsymbol{S}$, and $\boldsymbol{C}$ are the diffraction vectors of the primary, secondary, and coupling reflections, respectively. θ_G is the Bragg angle for the diffraction vector $\boldsymbol{G}$.

XRS consists in keeping the primary reflection excited while the crystal rotates around $\boldsymbol{P}$, named φ rotation. When secondary reflections are excited by the φ rotation, Eqs. (2) and (3) are fulfilled, and then the monitored primary intensity changes given rise to the $umwegs$. The most well known expression to predict $umweg$ positions in XRS were obtained from Eq. (2) [2, 3, 4, 5, 6] assuming that the primary reflection is always aligned, i.e. Eq. (1) fulfilled during a complete φ rotation of 360^o. It is therefore implicit in the standard equation of XRS, which is

$$\cos\beta = \frac{\sin\theta_S - \sin\theta_P\cos\gamma}{\cos\theta_P\sin\gamma}, \tag{4}$$

a perfect alignment between the diffraction vector $\boldsymbol{P}$ and the goniometer φ rotation axis, as shown in Fig. 1 where the angles β and γ are defined.

Recently, by using Eqs. (2) and (3) tiny deviations in the $umweg$ positions due to residual sample misalignments have been quantified [9]. It has shown that for primary reflections with four-fold symmetry axis the $umweg$ positions can be obtained free of sample misalignment errors, and that by measuring $umwegs$ owing to Bragg-surface diffraction cases the in-plane strains regarding two orthogonal directions are determined very accurately.

At the achieved level of accuracy, uncertainties in measuring positions of peaks presenting asymmetric profiles start to be significant. $Umwegs$ are sensitive to the invariant phase of structure-factor triplets, and then, even those cases related by axial symmetry, i.e. cases of a same family, will present different profiles when anomalous dispersion effects are not negligible. A relatively simple line-profile function has been

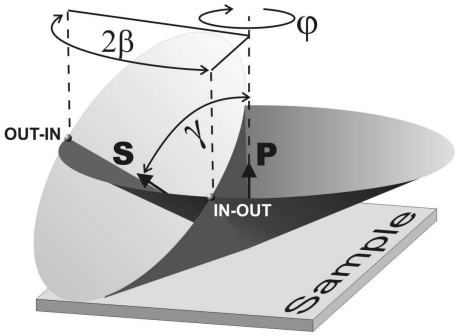

Fig. 1 Bragg cones of primary and secondary reflections, diffraction vectors $\boldsymbol{P}$ and $\boldsymbol{S}$, respectively. $\boldsymbol{P}\cdot\boldsymbol{S} = |\boldsymbol{P}||\boldsymbol{S}|\cos\gamma$. In a complete φ rotation of 360^o, the secondary reflection is excited twice, at φ_1 (*out-in*) and φ_2 (*in-out*) positions for a clockwise crystal rotation sense. The angular distance $2\beta = \varphi_2 - \varphi_1$, between these two positions can be calculated by Eq. (4) when $\boldsymbol{P}$ is perfectly aligned to the goniometer φ rotation axis.

Sample (#)	BUFFER (nm)	QDs (density)	CAP (nm)
1	–	–	–
2	200	–	–
3	200	high	–
4	200	low	–
5	200	high	30
6	200	low	30

Table 1 Details of the investigated samples. All substrates are adjacent pieces of a same GaAs (001) wafer, GaAs buffer and cap layers were growth by molecular beam epitaxy, as well as the 2.4 monolayers of InAs used to form the QDs. Low and high densities of QDs stand to growth ratios of 0.007ML/s and 0.09ML/s, respectively. Samples #3 and #4 are identical to samples #5 and #6, expect that they were removed from the growth sequence prior to the cap-layer deposition. The last two samples were covered in a single run, i.e. same cap-layer.

used to fit the $umwegs$ for phasing purposes [12]. To be applied here in peak position measurements that function can be simplified to

$$I(\varphi) = \{|D_1|^2 + |D_2(\varphi)|^2 + \xi D_1 D_2^*(\varphi) + \xi D_1^* D_2(\varphi)\} * G(\varphi) \tag{5}$$

where the intrinsic profile is given by

$$D_2(\varphi) = R\frac{w_{\rm S}}{2(\varphi-\varphi_0) - iw_{\rm S}}e^{i\delta_T} \tag{6}$$

which includes the $umweg$ peak position at φ_0, its invariant phase triplet δ_T, its relative strength R^2 regarding the base-line intensity $|D_1|^2$, i.e. the primary intensity, and the intrinsic width w given in $w_{\rm S} = \pm w$ where the $+$ and $-$ signals stand for *out-in* and *in-out*, respectively. A convolution with a gaussian function $G(\varphi)$, of fwhm $w_{\rm G}$, accounts for both mosaicity and instrumental broadening. The last adjustable parameter $\xi \in [0,1]$ is physically related to crystalline perfection, but here its is used just to tune the peak asymmetry. It provides a great flexibility in guessing a value for the invariant phase δ_T, if unknown, since there are strong correlations among the R, ξ, and δ_T parameters, as extensively discussed elsewhere [12].

3 Experimental details

From a commercial GaAs (001) wafer to samples with single-buried InAs QDs, the growth sequence by molecular beam epitaxy has been deposition of 200nm thick layer of GaAs (buffer), 2.4 monolayers of InAs to form the QDs, and 30nm GaAs layer (cap). As summarized in Table 1, the investigated series of samples represent different stages of this growth sequence for samples with low and high density of QDs, as verified via atomic force microscopy on samples with exposed QDs, see Fig.2. X-ray diffraction data have been collected at the Brazilian Synchrotron Light Laboratory (LNLS) with the polarimeter-like diffractometer described elsewhere [13]. Both ω and φ goniometer axes have a minimum step width of 0.0002^o provided by rotation stages from HUBER Diffraktionstechnik GmbH & Co. KG, model 410 with gear reduction. Instrumental broadening has been minimized by closing tightly the vertical and horizontal white-beam and scattering slits at the station XRD1, a bending magnetic beam line with a two-bounce Si (111) monochromator. The nominal X-ray photon energy, i.e. the monochromator encoder ready-out value whose inaccuracy is about 2 eV in our case, was set to 9320.6 eV (nominal wavelength $\lambda = 1.330232$Å), and kept unchanged during acquisition of the whole data set.

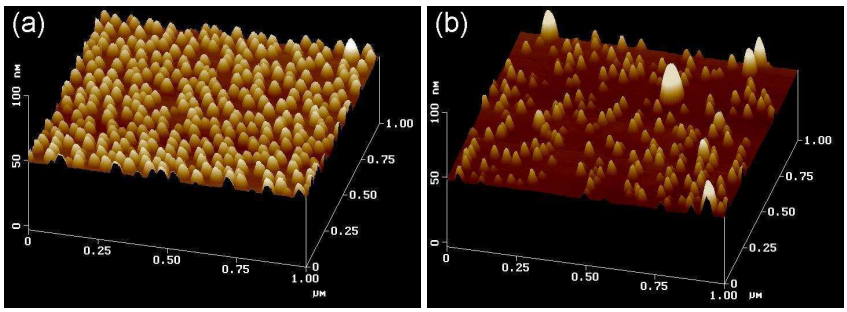

Fig. 2 Atomic force microscopy images of exposed QDs growth at ratios of (a) 0.09ML/s and (b) 0.007ML/s, samples #3 and #4 in Table 1. Density of QDs: (a) 360QD/μm^2 and (b) 200QD/μm^2. Average height: (a) 10 nm and (b) 8 nm. Average radius: (a) 26 nm and (b) 21 nm.

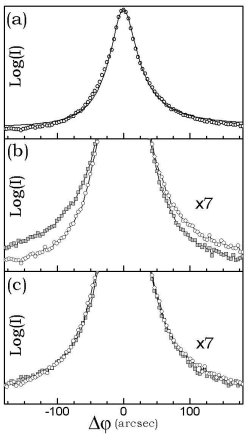

Fig. 3 Bragg-surface diffraction $umwegs$, $hk1$ type of secondary reflection with $h, k = \pm 1$. GaAs (001) wafer, sample #1. $\Delta\varphi = \varphi - \varphi_0$. (a) Experimental data (open circles) and best fitting curve (solid line) obtained via genetic algorithm [14]. (b) *out-in* (open circles) and *in-out* (gray squares) cases of the $umwegs$ with $\delta_T = 83.3^o$, and (c) with $\delta_T = -87.7^o$.

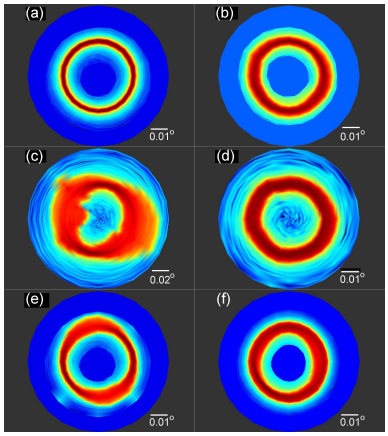

Fig. 4 Polar diagrams of the 002 GaAs reflection for samples #1 to #6, (a) to (f), respectively. Each diagram is composed by 25 rocking-curves of the 002 reflection, whose nominal Bragg angle is 13.61^o. Each curve was carried out with a step width of 0.001^o.

XRS were carried out on the 002 GaAs reflection, diffraction vector ***P***, in a vertical diffraction plane (σ polarization). Eight $umwegs$ have been measured, corresponding to the *out-in* and *in-out* positions of the four $hk1$ secondary reflections where $h, k = \pm 1$. The crystal $[110]$ in-plane direction was taken as reference for the φ rotation, i.e. $\varphi = 0$. To assure mechanical accuracy, the φ-scan data for this set of $umwegs$ were collected without changing the rotation sense of the φ axis. Rocking-curves of the 002 reflections at $\varphi = \varphi_0 - 0.1^o$ were carried out prior to each φ-scan to tune the incidence angle ω to the maximum of the primary reflection. All steps in this procedure have been repeated at least three times to each sample.

The peak position φ_0 of each $umweg$ was determined by fitting the φ-scan with Eq. (5) where the parameters w, R, ξ, w_G, and φ_0 have been adjusted via a genetic algorithm [14]. Typical values of best fittings are $w = 0.0088^o$, $R = 3.2$, and $w_G = 0.0015^o$. For the used x-ray photon energy, $umwegs$ with ***S*** projecting on the $[110]$ and $[\bar{1}10]$ in-plane directions have distinct invariant phase triplets, $\delta_T = -87.7^o$ and 83.3^o respectively. The former implies in nearly symmetric peaks while the other provides a perceptible asymmetry, as shown in Fig. 3. Since both invariant phases are in the range from -90^o to $+90^o$, the value of δ_T in Eq. (6) has been set to zero for all measured $umwegs$; it could be set to any value in this range, except the limiting values $\pm 90^o$ that would enforce symmetric profiles. Fitting the asymmetrical profiles with a symmetrical function, Eq. (5) with $\xi = 0$ or $\delta_T = \pm 90^o$, generates a shift in the peak position of the same order of our mechanical accuracy, i.e. of the order of 0.0002^o. It is important to emphasize that it is NOT necessary to calculate invariant phase values for peak position measurement purposes. In fact, δ_T could also be taken as another adjustable parameter limited either in the range $-90^o < \delta_T < +90^o$ or $+90^o < \delta_T < 270^o$ depending on the observed peak asymmetries, which will be reproduced for δ_T in only one of these ranges.

4 Results and Discussions

During sample alignment procedures, i.e. when aligning the diffraction vector ***P*** to the φ rotation axis, changes in the rocking-curves of the 002 reflection as a function of the azimuthal rotation has been observed, as characterized by the polar diagrams shown in Fig. 4. The growth of the buffer-layer has revealed

crystalline defects that would already exist in the surface of the commercial wafer prior to the growth, as can be inferred by comparing Figs. 4(a) and 4(b). Diffuse scattering increases for samples with exposed QDs, Figs. 4(c)and 4(d), being enhanced and anisotropic for the one with higher density of QDs, Fig. 4(c). Covering the QDs has eliminated their diffuse scattering, Figs. 4(e) and 4(f), but the anisotropy has propagated to the cap-layer, Fig. 4(e).

	$\bar{1}\bar{1}\bar{1}$		$\bar{1}1\bar{1}$		$\bar{1}11$		$1\bar{1}\bar{1}$	
	φ_1	φ_2	φ_1	φ_2	φ_1	φ_2	φ_1	φ_2
1	-85.085905	85.078201	94.903329	265.089485	4.902789	175.088778	184.913990	355.079471
2	-85.086165	85.078424	94.903241	265.089475	4.902523	175.088760	184.914026	355.079243
3	-85.086588	85.078551	94.903448	265.089739	4.902460	175.088701	184.913839	355.079396
β	85.082306±0.000258		85.093113±0.000034		85.093078±0.000063		85.082709±0.000085	
$\bar{\beta}$	85.087710±0.000146				85.087893±0.000074			
ν	$(6.33 \pm 0.43) \times 10^{-5}$				$(5.78 \pm 0.22) \times 10^{-5}$			

Table 2 Azimuthal φ positions of the 111, $\bar{1}\bar{1}1$, $\bar{1}11$, and $1\bar{1}1$ secondary reflections in the XRS of the commercial wafer, sample #1. Each position was measured three times (rows 1, 2 and 3) as explained in the text, $\beta = (\varphi_2 - \varphi_1)/2$, $\bar{\beta}$ are the average misalignment-free values, and ν stands for the unit-cell tetragonal distortion, Eq. (7). Angular values are given in degrees.

To evidence the sample misalignment effects on the φ-positions of the $umwegs$, sample #1 has been intentionally misaligned by about 0.02^o on both tilt axes of the goniometer head. Then, the maxima of the rocking-curves carried out at $\varphi = 0$ and $\varphi = 180^o$ differ by $\Delta\omega_{[110]} = \omega_{180} - \omega_0 = 0.0461^o$, and similarly $\Delta\omega_{[\bar{1}10]} = \omega_{270} - \omega_{90} = -0.0392^o$. The effects of such misalignments are thus observed when comparing in Table 1 the β values for the analyzed secondary reflections. It also shows that the average $\bar{\beta}$ values regarding each one of this in-plane directions are misalignment-free values with overlapping error bars.

The amount of in-plane strain ν has been calculated from Eq. (4) by assuming a tetragonal distortion of the unit cell so that $\boldsymbol{S} = (h/a, k/b, 1/c)$, $a = b = a_0(1-\nu)$, $c = a_0(1+2\nu)$, and

$$\beta(\nu) = \beta_0 + \nu \left(\frac{\partial\beta}{\partial\nu}\right)_{\nu=0} \tag{7}$$

where $\beta_0 = 85.089848^o$ and $(\partial\beta/\partial\nu)_{\nu=0} = -33.87^o$ for the nominal ratio $a_0/\lambda = 4.2499$. Fig. 5 shows the so measured in-plane strain to all samples described in Table 1. The ν values for samples #1 to #4 do not present a relevant variation since they are all in a narrow range from 5.3×10^{-5} to 8.7×10^{-5}, or $\nu = (7.0 \pm 1.7) \times 10^{-5}$, which could stand for a variation around a null strain if a slightly different ratio of $a_0/\lambda = 4.2480$ had been used instead of the nominal one.

Significant tetragonal lattice distortion, given here in terms of the in-plane strain ν, is observed only after covering the QDs. In sample #6, the one with low density of QDs, the strain value $\nu = (4.6 \pm 0.4) \times 10^{-5}$ already indicates a change towards an in-plane expansion of the unit cells; tendency that is furthermore clear in the case of sample #5, the one with high density of buried QDs. Its outrange expansive strain value of $\nu = (-184.1 \pm 1.3) \times 10^{-5}$ is also followed by visible changes in the intrinsic character of the $umwegs$, going from a lorentzian-like peak to a gaussian one, as can be seen in Fig. 6.

For the chosen Bragg-surface diffraction $umwegs$, very strong secondary and coupling reflections plus a secondary beam, wavevector $\boldsymbol{k}_S = \boldsymbol{S} + \boldsymbol{k}$, nearly parallel to the surface provide a shallower penetration depth than for the primary reflection, which is already impinging the surface at a low angle of about 13.6^o. The effective penetration depth (50% intensity reduction) in the GaAs crystal has been measured, for x-rays of 8keV, by means of longitudinal scan of the 002 rod in triple axis goniometry [11]. 150 nm and 1000 nm were the estimated values when the $umweg$ is excited and when the 002 reflection diffracts alone, respectively. Therefore, in both cases, the probing depth should not be limited within the 30nm

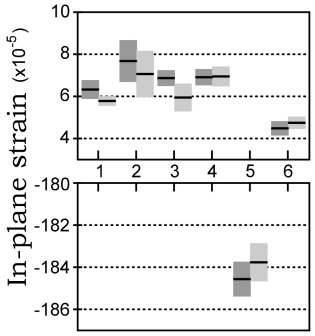

Fig. 5 Measured in-plane strain ν, along the $[110]$ (darker error bar) and $[\bar{1}10]$ (lighter error bar) directions for samples #1 to #6 as defined in Table 1.

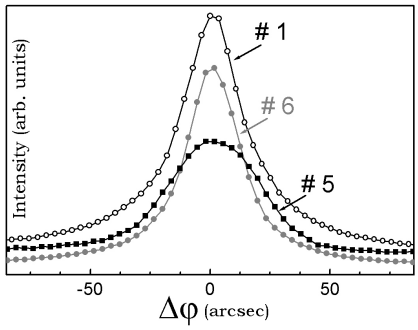

Fig. 6 Azimuthal profiles of the measured $umwegs$ for samples #1 (open circles), #5 (gray circles), and #6 (black squares). The intensity scales have been displaced for comparison purposes. $\Delta\varphi = \varphi - \varphi_0$.

thick cap-layer, and then, neither the strain induced by the growth of the cap-layer. In other words, the cap-layer growth has strained the substrate lattice in an amount that seems to be related to the density of QDs. Moreover, the gaussian-like profile of the $umwegs$ observed in sample #5 indicates that some mosaicity, i.e. crystalline defects, have been introduced at near the surface of this sample.

5 Conclusions

In this work, a systematic procedure for studying nanostructured semiconductor devices via XRS has been developed. It allows in-plane surface strains to be determined in two orthogonal directions with an accuracy below 10^{-5}. Covering InAs QDs growth on GaAs (001) substrates generates an expansive in-plane strain that is related to the density of QDs. As an unexpected result, it has been shown that rocking curves of the 002 GaAs reflection are sensitive to crystalline perfection of the buffer-layer, as well as to the diffuse scattering of the QDs. Polar diagrams of this reflection can therefore be an useful tool to inspect the quality and in-plane anisotropy of the growths.

Acknowledgements This work was supported by the Brazilian founding agencies FAPESP (proc. No. 02/10387-5), CNPq (proc. No. 141369/2006-0 and 301617/95-3), and LNLS (under proposals D12A-XRD1-4733 and AFM-4614).

References

[1] M. Renninger, Z. Phys. **106**, 141–176 (1937).
[2] H. Cole, F. W. Chambers and H. M. Dunn, Acta Cryst. **15**, 138–144 (1962).
[3] S. Caticha Ellis, Acta Cryst. A**25**, 666–673 (1969).
[4] B.J. Isherwood and C.A. Wallace, Acta Cryst. A**27**, 119–130 (1971).
[5] F.J. Spooner and C.G. Wilson, J. Appl. Cryst. **6**, 132–135 (1973).
[6] S.L. Chang and B. Post, Acta Cryst. A**31**, 832–835 (1975).
[7] L.H. Avanci, L.P. Cardoso, S.E. Girdwood, D. Pugh, J.N. Sherwood and K.J. Roberts, Phys. Rev. Lett. **81**, 5426–5429 (1998)
[8] M.J. da Silva, A.A. Quivy, S. Martini, T.E. Lamas, E.C.F. da Silva, and J.R. Leite, Appl. Phys. Lett. **82**, 2646–2648 (2003).
[9] S.L. Morelhão, L.H. Avanci, R. Freitas and A.A. Quivy, Microelectron. J. **36** 219–222 (2005)
[10] S.L. Morelhão and L.P. Cardoso, J. Appl. Cryst. **29**, 446–456 (1996).
[11] S.L. Morelhão and E. Abramof, J. Appl. Cryst. **32**, 871–877 (1999).
[12] S.L. Morelhão, L.H. Avanci and S. Kycia, Nucl. Instrum. Meth. B **238**, 175–184 (2005).
[13] S.L. Morelhão, J. Sync. Rad. **10**, 236–241 (2003).
[14] M. Wormington, C. Panaccione, K. M. Matney, D. K. Bowen, Phil. Trans. R. Soc. Lond. A**357**, 2827–2848 (1999).